Human Cryptochrome Mediates Oxidative Stress Responses Modulated by Static and Electromagnetic Fields in Doxorubicin-Treated Cells

Behnam Hajipour-Verdom
Tarbiat Modares University
Mozhgan Alipour
Tarbiat Modares University
Parviz Abdolmaleki (parviz@modares.ac.ir)
Tarbiat Modares University
Saman Hosseinkhani
Tarbiat Modares University
Mehdi Khoobi
Tehran University of Medical Sciences
Zahra Panjali
Shahid Beheshti University of Medical Sciences
Mohsen Alipour
Jahrom University of Medical Sciences
Nader Riyahi Alam
Tehran University of Medical Sciences

Research Article

Keywords: Cryptochrome, Static magnetic field, Electromagnetic field, Doxorubicin, Cellular responses.

Posted Date: December 29th, 2020

DOI: https://doi.org/10.21203/rs.3.rs-132719/v1

Abstract

Cryptochromes (CRYs) have been suggested to involve in the magnetic sensing for navigation of migratory birds in response to Earth's magnetic fields. Magnetic fields (MFs) through wireless penetration change the cell physiology by effect on physicochemical reactions. Here, we aimed to investigate the behavior of HEK 293T cells overexpressing human CRY-based magnetoreception complexes undergo doxorubicin (DOX) treatment and exposure to moderate intensity static magnetic field (SMF) and extremely low frequency-pulsed electromagnetic field (ELF-PEMF). The ability of this magnetosensor is depended on CRY-photoreceptor proteins that complemented with putative magnetosensor proteins (MagR). The results indicate that magnetic sensitivity of CRY-based magnetosensor can effects on the intracellular reactive oxygen species (ROS) production and cell growth, cell cycle progression and expression of DNA damage-related genes due to treatment of DOX, SMF and ELF-PEMF. Our findings show that ROS accumulation significantly decreased in the cells expressing CRY/MagR complexes in response to all treatments, and also cell viability is decreased in contrast to MFs exposure. In addition, magnetosensitive complexes mediated the upregulation of genes in the base excision repair (BER) pathway including ITPA in presence of SMF as well as MTH1 in presence of ELF-PEMF in the DOX treated-cells. Furthermore, CRY/MagR induced a remarkable cell cycle arrest at G0/G1 phase in the all treatments. These results demonstrated that CRY/MagR complexes modify the DNA damage responses during genotoxic stresses by controlling the cell cycle progression and ROS levels. Therefore, our data suggest that CRY-based magnetosensitive complexes can increase the cytotoxic effects of DOX even when SMF and/or ELF-PEMF exposure were provided, exclusively.

Introduction

Magnetic fields (MFs) have non-invasive penetration to deep tissues of living system and wirelessly interact with biological components, but it is largely unknown that how the MFs influence on the parameters of cell behaviors such as cell growth and change the cell contexts[1,2]. MFs have more applied in the medicine like MRI diagnostics, magnetoencephalography, etc[3]. However, some studies indicated that exposure to MFs increases the production of deleterious free radicals and their pathological effects upon human health as possibly carcinogens, which could cause some cancers like childhood leukaemia[4,5].

MFs can be classified the static magnetic fields (SMF) in various intensity ranges including week (< 1 mT), moderate (1 mT-1 T) and high (1 T <), and also electromagnetic field (EMF) in various frequency including extremely low-frequency (< 300 Hz), intermediate (300 Hz-10 MHz) and radiofrequency (10 MHz-300 GHz)[6,7]. Moreover, pulsed EMF (PEMF) represent a sub-class of EMFs containing frequencies from 6 Hz up to 500 Hz[8,9]. The disparate influences of SMF and EMF stimulation on the living organisms were explained in the well-known theory as Window Effect, which is depended on the direct and indirect effects of multiple factors including physical concepts of MFs such as intensity, frequency, pattern, exposure time and sources, and also biophysicochemical properties of biological

target like type of cells in the bacteria, plant and animals, etc[10,11]. Externally applied MFs increase the lifetime and production of free radicals and their reactivity rates in cells undergo physicochemical mechanisms comprising intramolecular electron-nuclear hyperfine structures, Zeeman Effect, singlet/triplet interconversion states, Fenton and Haber-Weiss reaction, etc.,[12–14].

The Earth's natural magnetic fields consist of quasi-SMF at low intensity ~ 50 μT, and also extremely low frequency-PEMF (ELF-PEMF) ~ 7.83 Hz known as Schumann resonance. Some animal species can sense the geomagnetic fields (GMF) to enable behaviors including navigation and migration, growth and reproduction, etc[15]. Studies proposed that cryptochrome (CRY)-based magnetic compass senses the GMF underlying a magnetically sensitive chemical reactions[16,17]. CRYs are a family of highly conserved flavoproteins involving electron transfer and redox-active flavin adenine dinucleotide (FAD) that respond to UV-A/blue light and MFs as identified in the all biological kingdom from bacteria to plants and animals to humans[18–20]. FAD cofactor is photo-sensitive that reduced from an oxidized form to an anionic semiquinone ($FAD^{\bullet-}$) state under light exposure[21,22]. Mammals have two family members of CRYs that expressed in the suprachiasmatic nucleus (SCN) as well as in the many other tissues, which are necessary in the normal circadian rhythms and molecular clock mechanisms that mediate the electrophysiological depolarization, action potential and resting in the SCN and optic nerves in response to daylight and GMF[23–25].

The circadian clocks control the various daily rhythmicity of the biochemistry, physiology, and behavioral processes in mammals[26]. Moreover, the circadian cycle may influences the efficiency of cancer chemotherapy that known as chronochemotherapy, through modification the cytotoxicity of anticancer drugs and pharmacokinetics parameters in the tumors[27]. Some evidences indicated that MFs have different effects on the cancer development, which may depend on the exposure parameters[10]. Moreover, some studies demonstrated that long-term exposure to EMF can limits the cytotoxicity effects of chemotherapeutics[28,29]. MFs may lead to therapeutic effects on the cancer cells by modulating cell cycle events, DNA repair responses and circadian rhythms[30]. In addition, studies have shown that EMF exposure can cause to disruption in the memory and neural-like behaviors, intracellular signaling cascades, etc., by affecting on the circadian rhythms and molecular clock in the animals specially mammals and insects[31,32]. The mechanisms of MFs-interactions within living systems such as human exposure are a fascinating biological challenge and unclear. However, the effects of MFs have been widely discussed as physical stimuli or inhibitors.

Doxorubicin (DOX) is a natural-product anthracycline antibiotic used as a chemotherapy agent for a broad spectrum of solid tumors that is limited due to some side effects and drug resistance[33]. DOX mainly triggers the cell death through stimulation of DNA damages and disruption of DNA repair, which is because of double-strand breaks by inhibition of topoisomerase II and oxidative stresses through generation of intracellular reactive oxygen species (ROS) against tumor cells[34]. In addition, DOX has more adverse effects in the many additional cellular functions involving ceramide metabolism, cell cycle arrest, etc[35]. Studies demonstrated that cells activate multiple repair mechanisms to detect and repair the

DOX-induced DNA damages[36]. Many studies showed that DNA topoisomerases play a role in the regulating of DNA topological changes, and induce either single- (type I) or double- (type II) strand DNA breaks. These enzymes regulate the gene expression in the circadian system, so that the inhibition of them can lengthen the circadian periods[37,38].

ROS have essential pleiotropic roles in the various cellular functions, including redox signaling at homeostasis and physiological levels or deleterious effects at pathological levels[39,40]. ROS are associated in inflammation-related disorders such as aging, asthma, cancer, diabetes, neurodegeneration, etc[41]. Oxidative stress leads to DNA damages in the both nuclear and mitochondrial genomes of cells[42]. Cells have defence mechanisms that are activated in response to ROS/oxidative stress signaling, including anti-oxidants scavengers containing glutathione (GSH), glutathione peroxidase (GPx), catalase (CAT), superoxide dismutase (SOD), etc., and also DNA damage responses (DDR)[43,44]. DDR comprises the activation of multiple checkpoints, cell cycle arrest and DNA repair pathways that eventually outcomes either repair and cellular proliferation or apoptosis and cell death[45,46]. Oxidation events lead to promote the upregulation of DNA repair genes, mainly base excision repair (BER) pathway and also nucleotide excision repair (NER) and mismatch repair (MMR) pathways to deal with the detection and repair of oxidative DNA lesions[47,48].

MFs could cause oxidative damages by indirect interaction of ROS in the cellular components such as nucleic acids, proteins and lipids[49–51]. Studies have shown that MFs induce detectable cytogenotoxic effects and cell cycle arrest that interference into DNA repair mechanisms and may trigger the ferroptosis, necrosis and apoptosis cell-death in the normal and cancer cells[4,52]. Furthermore, studies indicated that CRYs as core components of circadian clock involve in the control of cell cycle and responses to DNA damages in mammalian cells[24,53].

In this study, we have analyzed the cell behaviors comprising cell cycle and capacity of BER pathway in the HEK 293T cells overexpressing the CRY-based magnetoreception complexes in response to oxidative stresses. Our aim was to investigate the regulating aspects of magnetosensitive proteins on the cellular responses to genotoxic stresses and possible links between the gene expression of BER pathway and oxidative DNA damages which were modulated by DOX, SMF and ELF-PEMF exposure (Fig. 1). Our findings demonstrate that CRY-based magnetosensor induces remarkable effects on the ROS accumulation and BER activity, and furthermore cell growth and viabilities and eventually boosts the efficiency of DOX-cytotoxicity even in exposure of MFs.

Results

CRY/MagR overexpression decreased intracellular ROS accumulation

The total intracellular ROS formation in the HEK 293T cells expressing either GFP or CRY/magnetosensor protein (MagR) genes under both DOX treatment (0.1 μM) and exposure of 10 mT SMF and 50 Hz ELF-PEMF was determined using 2',7'-dichlorofluorescein diacetate (DCFDA). As shown in Fig. 2, ROS levels significantly decreased in the CRY/MagR-expressing HEK 293T cells in the presence and absence of SMF, ELF-PEMF and DOX compared to sham. However, DOX, SMF and ELF-PEMF treatments induced significant increase of ROS production in the other cell treatments. A clear distinction could be observed between cells with overexpression of CRY/MagR and other groups in the ROS accumulation in the presence and absence of MFs (Fig. 2c,d).

CRY/MagR induced G0/G1 phase cell cycle arrest

The distribution of GFP- and CRY/MagR-expressing HEK 293T cells following treatment with DOX (0.1 μM) in exposure of SMF (15 mT) and ELF-PEMF (50 Hz) at different phases of cell cycle were analyzed using propidium iodide (PI) and flow cytometry (**Supplementary Fig. S1**). As shown in Fig. 3a, although the arrest was not statistically significant in the cells at the endpoint of transfection, but a typical G0/G1 cell cycle arrest pattern was observed in GFP- and CRY/MagR-expressing HEK 293T cells at 24 h afterthat compared to control cells (Fig. 3b). Notably, DOX caused G2/M phase arrest in all of non-CRY/MagR-expressing HEK 293T cells after 24 h treatments, and furthermore when was accompanied by a decrease in the number of cells at G0/G1 phase in presence and absence of SMF compared to S phase in ELF-PEMF treatments relative to sham, respectively (Figs. 3b,c,d). The proportion of G0/G1 phase arrest was substantially increased in the CRY/MagR-expressing cells, which was accompanied by a decrease in the cell accumulation in S phase and G2/M phase except for combination treatments of SMF and DOX at S phase relative to sham (Figs. 3c,d). In addition, ELF-PEMF exposure induced G0/G1 arrest with a decrease in the cell number at S phase and G2/M phase, while these trends were not noticeable in presence of SMF. These results suggested that CRY/MagR-based magnetosensor can modulate cell growth in response to MFs through inhibition of G0/G1 to S phase transition in the cell cycle.

Effects of SMF, ELF-PEMF and DOX on cell growth of CRY/MagR complex-expressing cells

We assessed the cell viability of HEK 293T cells expressing either GFP or CRY/MagR treated with 0.1 μM DOX in exposure of 15 mT SMF, 50 Hz ELF-PEMF through MTT staining and microplate reader. Cell viability significantly decreased in the DOX-treated wild-type and GFP-expressing HEK 293T cells compared to control cells (Fig. 4a). As shown in Fig. 4b,c, both SMF and ELF-PEMF induced the proliferation in the wild-type HEK 293T cells compared to sham. However, the viability significantly decreased in the cells expressing either GPF or CRY/MagR genes in all treatments.

CRY/MagR modulated expression of oxidative stress-responsive genes

To determine the effects of DOX (0.1 μM) upon HEK 293T cells expressing either GFP or CRY/MagR genes in exposure of SMF (15 mT) and ELF-PEMF (50 Hz) that stimulate the ROS production, we quantified the mRNA expression levels of oxidative stress-responsible genes including OGG1, MTH1, ITPA in the BER DNA repair pathway using qRT-PCR analysis. As shown in Fig. 5a, all three of these genes showed statistically significant decreased expression in cells expressing CRY/MagR at the endpoint of transfection compared to 24 h after that expression level of ITPA gene significantly increased in absence of MFs compared to control cells (Fig. 5b). As can be seen in Fig. 5c, SMF significantly induced the expression of MTH1 gene in the CRY/MagR-expressing HEK 293T cells, and also levels of ITPA gene expression showed significant enhancement in response to SMF and DOX in the wild-type and CRY/MagR-expressing cells. Furthermore, combination treatments with DOX more than just SMF, significantly boosted the levels of ITPA expression. ELF-PEMF exposure significantly decreased the levels of OGG1 gene expression in the wild-type and CRY/MagR-expressing HEK 293T cells, and also decreased the levels of ITPA expression in all cell groups compared to sham (Fig. 5d). In addition, MTH1 expression interestingly showed significant decreased in CRY/MagR-expressing HEK 293T cells compared to significant increase in the wild-type cells in response to ELF-PEMF and DOX treatments. Combination treatments with DOX enhanced the expression levels of MTH1 more than SMF alone compared to sham. These results indicated that different biological activities of BER activity as response to ROS-modulators has been observed from CRY-based magnetosensor.

Discussion

Although this is still unknown that whether migratory birds and many other animals can detect the variations of Earth's magnetic fields, and used for orientation and navigation behaviors, but the best explain is suggested as possible biophysical model underlying radical pair-based mechanism in a protein biological compass[17]. These rod-like shaped magnetosensor complexes is related to couple of CRY-photoreceptor with magnetosensitive MagR proteins, which is roughly confirmed by experimental and theoretical foundations in the bacteria, animals, etc[16]. Here, we investigated the possible impacts of human's CRY/MagR-based magnetoreception complexes in response to ROS accumulation of DOX-treated HEK 293T cells in exposure of SMF and ELF-PEMF due to cell physiological function and behaviors such as cell cycle and DNA repair responses.

Humans are continuously exposed to MFs, which are from natural origin comprising GMF, thunderstorm, solar storms and/or manmade sources such as power transmission lines, factories, MRI and other therapeutic apparatuses, etc[54]. Indeed, MFs as stimuli or deleterious stresses are important phenomena in our surrounding environment, has been associated with the human health modulate the physiological and hemostatic functions of cells especially neural cells and the circadian periods[55,56]. However, the mechanism of these biologic influencing is not well-established on the cellular behaviors.

Many biological systems are enabled adaptation and respond to GMF and various artificial MFs by some possible proposed-mechanisms, which integrate and convert the wireless physical information of MFs to chemical and physiological signals in the cell behavior and responses. First mechanism involves a

mechanically sensitive ferrimagnetic or superparamagnetic iron-containing particles-based magnetosensor like a miniature compass needle, the second an electromagnetic induction in the accessory proteins and others is based on light-sensitive radical pair mechanism[16,57–59]. Following the last reported, CRYs are the best candidate for biochemical magnetoreceptor that mediate light-dependent magnetosensitivity with radical-pair reaction, which associated with $FAD^{-\circ}$ binding to CRY-photoreceptor proteins[16,19]. Furthermore, some recent experiments revealed that radical pair formation in the mammalian-type CRYs can occurs during magnetosensitivity by molecular oxygen and is not dependent to light[60–62]. CRYs can implicate to reinnervation and repairing of nervous systems in the mammalian brain as light-independent magnetosensor by an external low intensity EMF stimulations[63]. However, magnetosensitivity property requires the light in the flies, birds, etc.

In the current study, we used a moderate intensity SMF of 15 mT that is about 300X the very week intensity of GMF (~ 50 μT) and also 50 Hz ELF-PEMF which is around 6X the Schumann resonance (~ 7.83 Hz) upon cells overexpressing CRY-based magnetoreception complexes. We analyzed that whether these MFs effect on the cell cycle events and DNA repair mechanisms. Circadian clock implicates to modify the many physiological functions in mammals including metabolism, cell cycle and DNA damage responses, cell growth and survival, apoptosis and angiogenesis, immune system and cellular senescence, etc[64–66]. Some studies showed that the disruption of human circadian clock leads to failures in the control of the cell cycle mechanisms, and increased the cancer risk[67]. In contrast, circadian system can protects tumor cells from chemotherapeutics. Therefore, CRYs play a pleiotropic role in the cells such related to p53 activity and cell cycle progression, and also DNA damage pathways, etc[62,68].

Studies have shown that the overexpression of CRYs in numerous neuronal cells increases the effects of MFs exposure on the cell behaviors and neural activities[63,69]. Redox cycling of CRYs participates the formation of radical pair and singlet/triplet interconversion in the $FAD^{-\circ}$ that triggers the transfer electron form CRYs to MagR and magnetic susceptibility in MagR proteins[16]. In addition, redox cycling leads to H_2O_2 and other ROS production in exposure of MFs and light[60,70]. In the present study, the physical and chemical treatments cause to ROS production, but overexpression of magnetosensitive complexes decreased the ROS accumulation in the treated-cells (Fig. 2). Following recent study by Sherrard et al., that showed human CRY-transformants can sense 10 Hz low-intensity EMF which decreased the intracellular ROS levels in the human cells, and also suggesting that human CRY2 is as considered blue light-responsive mediator[60].

To further investigate, we evaluated the cell growth, cell cycle progression, and DNA repair capacity. Circadian cycle and cell cycle are two interdependent important regulatory mechanisms that directly or indirectly impact on the physiological and biochemical reactions, and also determine the behavior and fate of cells[71]. We found that CRY/MagR overexpression can changes the cell distribution and triggers the cell cycle arrest in the G0/G1 phases and consequently boosted the cytotoxicity of DOX in presence of SMF and ELF-PEMF (Figs. 3, 4). Indeed, although DOX alone induced G2/M phase cell cycle arrest and decreased the cell viability, but 50 Hz ELF-PEMF exposure may changes the transition acceleration of

G2/M to G0/G1 phases, thereby led to G0/G1 phase cell accumulation and increase of cell proliferation. However, SMF did not show any significant effects on the cell cycle progression, but similarly increased the cell viability. Probably, transition acceleration of G2/M to G0/G1 phases occurred in the combined treatments of DOX via SMF or EMF that didn't show any significant cytotoxic effects.

When DNA is exposed to oxidative stresses, damages occur in the bases and sugar of some sensitive nucleotides like guanine and lead to forming the side-products such as 8-oxoguanine (8-oxoG)[72]. The 8-oxoG displays mutagenic potential by inducing GC-TA transversion in the DNA replication[73]. Some DNA repairing mechanisms including MMR, BER and NER pathways generally implicate in response to ROS/RNS-induced DNA damages[74]. However, BER is therefore the main repair system, removes a wide range of oxidative DNA-damaged bases[75]. We eventually examined that whether the circadian clocks change the oxidative damage-responsible gene expression of 8-oxoguanine DNA glycolysis (OGG1), human mutt homolog 1 (MTH1) and inosine triphosphate pyrophosphate (ITPA) in the BER pathway. These enzymes directly and indirectly recognize and cleave the 8-oxoG adducts, comprising OGG1 in the DNA double helix and also MTH1 and ITPA in the nucleotide pools[76–78]. Studies showed that UV-damaged DNA can repair by DNA photolyases of CRY, which is depended on blue light induction[79]. In addition, findings confirmed that the circadian clocks may optimize the repairing DNA lesions by NER and MMR pathways[80–82].

Some human health studies about the OGG1 gene expression didn't show any upregulation in response to oxidative DNA damages[72]. Interestingly in our study, exposure to DOX, SMF and EMF did not also upregulate the OGG1 in response to oxidative stresses, even during combined treatments (Fig. 5). Furthermore, our results suggest that ITPA more implicated in response to SMF oxidative damages, and MTH1 in EMF DNA repair responses of cells even when treated with DOX. We also noted that although SMF upregulated the MTH1 and ITPA in the cells overexpressing magnetosensitive complexes, EMF downregulated the all of our considered-genes in the BER capacity (Fig. 5c,d).

In conclusion, from a chronochemotherapy prospective, our work shows that exposure to high levels of external SMF or EMF relative to GMF change the physiological responses and repair mechanisms in cells which treated with chemotherapeutics such as DOX. So that, MFs may disrupt the efficiency of anticancer drugs. GMF in our surrounding environments has important complexity effects on the physiology and function of cells such action potential firing in the neural cells. By contrast, artificial-MFs cause to appear the neurodegenerative diseases in exposure of modern technology[83]. There are associations between CRY magnetoreception proteins with intracellular ROS accumulation, cell cycle and cellular repair responses in the course of SMF- and ELF-PEMF-induced pathology. Taken together, our findings demonstrate the relationship between the circadian rhythms and oxidative DNA damages while CRYs may control the BER activity by modifying the levels of cell cycle progression and ROS accumulation in response to SMF and EMF. Furthermore, our data suggest that although the therapeutic effects of DOX may modulated by SMF and EMF and also decreased cytotoxicity, but overexpression of magnetosensitive proteins could increase the efficiency of DOX-toxic effects when cells co-treated with

SMF or EMF. In addition, our study shows that magnetogenetic effects of ELF-PEMF (~ 6X GMF) were higher than SMF (~ 300X GMF) on the cell cycle events and gene expression. Based on the interference effects of MFs, future work may involves studying the influences of ELF-PEMF or SMF exposure on the neuroregeneration and repair due to magnetosensitive proteins and chronotherapeutics.

Methods

Molecular biology

The genes of human wild-type CRY 2, variant 2 (CRY2-2; NM_001127457.2) and MagR (NM_030940.3) that are necessity for the formation of magnetosensor complexes[16], were obtained from MCF-7 cell line. In brief, total RNA samples were isolated from cells using a RiboEx reagent (GeneAll, Korea). For cDNA synthesis, reverse transcription PCR was performed using Prime Script II reverse transcriptase (Takara, Japan) and two specific oligonucleotide primers were designed by oligoanalyzer software, and were synthesized by Pishgam Biotech Co. (Tehran, Iran). The complete open reading frame of CRY2-2 and MagR were amplified using forward (Fwd) and reverse (Rev) primers, which contained a restriction site (underlined) as followed:

CRY2-2-Fwd, 5'-CTAGCTAGCATGCCAGCTCCACCCGGGCG-3', Nhe1 restriction site;

CRY2-2-Rev, 5'-AAAGAGCTCTCAGGCATCCTTGCTCGGCA-3', Sac1 restriction site;

MagR-Fwd, 5'-CTAGCTAGCATGTCGGCTTCCTTAGTCCGG-3', Nhe1 restriction site;

MagR-Rev, 5'-AAAGAGCTCTCAAATATTAAAGCTTTCTCC-3', Sac1 restriction site.

We designed primers for PCR and resequencing the first exon of CRY2-2 that was incomplete in genome assembly, to achieve the full DNA coding sequence.

Construction of CRY and MagR expressing plasmids

The CRY2-2 and MagR cDNA were cloned into pDB2 (Invitrogen) as a high copy-number plasmid with kanamycin resistance cassette. The pDB2 vector was extracted using Qiagen Midi kit (Qiagen, Hilden, Germany). The DNA sequences and plasmid were double digested with Nhe1 and Sac1 restriction enzymes at 37 °C overnight, and thus gel purified. After that, the purified PCR fragment was ligated to the pDB2 vector by T4 DNA ligase at 14 °C overnight. In order to transform the recombinant DNA into *E. coli DH5α* competent cells, which were freshly prepared by calcium chloride ($CaCl_2$) treatment. Next, resulting recombinant DNA was transformed to *E. coli DH5α* according to the protocol. Cells were first grown overnight at 37 °C in LB media, and this starter culture was subsequently diluted 1:100 into LB media. The native pDB2 plasmid containing green fluorescent protein (GFP) followed an identical culturing approach. Clones were confirmed for correct insertion by restriction double digestion of the isolated plasmids (with Nhe1 and Sac1) and colony PCR. All plasmids were constructed by standard molecular

biology procedures and subsequently verified using an automatic sequencer (MWG) by cytomegalovirus (CMV) promoter and SV40_PA_terminator universal primers.

Cell culture

The MCF-7 human breast adenocarcinoma and human embryonic kidney 293T (HEK 293T) cell lines were used, originally obtained from National Cell Bank of Iran (NCBI) at Pasteur Institute of Iran (IPI). The cells were grown in Dulbecco's modified eagle's medium (DMEM) with neutral pH (7.2–7.4), containing 10% (v/v) heat-inactivated fetal bovine serum (FBS), L-glutamine (2 mM), 1% penicillin/streptomycin (all from Gibco). Cultures were maintained in a humidified incubator at 37 °C and 5% CO_2 atmosphere. The cell media was changed every 2–3 days, and when cells were confluent about 70–80%, they were trypsinized with 0.025% trypsin-EDTA (Bioidea, Iran). After attaching overnight, the cultivated cells were prepared to transfection.

Transfection

HEK 293T cells were stably transfected with vectors of pDB2_CRY2-2, pDB2_MagR and native GFP-expressing pDB2 plasmid as previously described. Transfection was achieved using 25 kDa branched polyethylenimine (bPEI25, Sigma-Aldrich) at a concentration of 3.57 mg PEI per mg plasmid DNA (pDNA)[84]. Briefly, 200×10^3 cells were seeded in six-well cell culture plates (SPL Life Sciences Co., Ltd. Korea) and incubated in a humidified atmosphere at 37 °C under 5% CO_2, overnight. Before transfection, polymeric nanoparticles (containing PEI and prepared-pDNA) were prepared and diluted in FBS-free DMEM in a total volume of 100 µl. At transfection time, the culture media was completely aspirated from the wells and replaced drop-wise with suspension of nanoparticles. After that, the supplemented DMEM with 10% FBS and 1% penicillin and streptomycin was added at 4 h later and cell culture plates were returned to the 37 °C incubator for 48 h to allow gene expression. As seen in **Supplementary Fig. S2**, the overexpression of these genes don't show significant toxic effects on the cells. The transfection efficiency was measured in cells, which were generated in the same way to express enhanced-GFP using a luciferase assay. Luciferase activity was measured by luminometer (Berthold detection systems, GmbH, Germany) at different times, and presented as relative light units (RLU/sec) per number of cells. As shown in **Supplementary Fig. S3**, maximum transfection efficiency was at 48 h post-transfection.

Characterization of nanoparticles

Gel retardation assay

The stability of DNA-binding polymeric complexes (PEI/pDNA) were examined by gel retardation assay as shown in **Supplementary Fig. S4**. The formation of electrostatic binding between the amine group of PEI with positive charge and phosphate group of DNA neutralize the negative charge of pDNA. Briefly, the complexes were prepared at defined concentration of 3.57 µg PEI and 1 µg pDNA. The complexes and free pDNA were loaded onto agarose gels (1%) and electrophoresed at 90 V for 50 min. The retardation of plasmid mobility was visualized by ethidium bromide (0.1 mg/ml) and ultraviolet imaging system.

Particle size and charge analysis

The particle size and zeta potential of each sample were measured by a Malvern Nano ZS instrument and DTS software (Malvern Instruments, UK) at room temperature. The samples were prepared at concentration of 3.57 µg PEI and 1 µg pDNA in cold PBS up to 1 ml. The results were analyzed by Zetasizer software (V6.12) as shown in **Supplementary Table S1**.

Cell treatments

The prepared-HEK 293T cells were treated by 0.1 µM DOX (Accord Healthcare) in exposure of 15 mT SMF and 50 Hz ELF-PEMF. In brief, cells were seeded into cell culture plates (SPL Life Sciences Co., Ltd. Korea) containing supplemented DMEM with 10% (v/v) FBS, 2 mM L-glutamine, 100 units/mL of penicillin and 100 mg/mL of streptomycin at 37 °C and 5% CO_2, respectively. Cells were initially allowed to attach overnight and then prepared for transfection by clonal plasmids containing either CRY and MagR or GFP. Afterward, the media was removed and treated by new supplemented DMEM in the DOX, sham- and SMF- or ELF-PEMF-exposed conditions for 24 h post-transfection. Generally, cells were characterized at the endpoint of transfection processes and 24 h after that.

Magnetic field exposure system

Exposure to SMF (15 mT) and ELF-PEMF (50 Hz) were used in this study that prepared by a locally designed homogeneous MF-generator. This platform consisted of two coils (1800 loops of 3.0 mm diameter coated copper wire), which were resistant to heat up to 200 °C through passing either direct current (DC) switching power supply or alternating current (AC) **(Supplementary Fig. S5a)**. Wirelength in each coil was about 1 km and each coil weighed approximately 40 kg. The coils received DC voltage up to 50 V and AC voltage 220 V and 50 Hz frequency, current up to 16 A, and the maximum provided-power was equal to 800 W. Coils had a total resistance and inductance of 3 Ω and 2 Henry, respectively. The electric power was provided using a 220 V/AC power supply equipped with a variable transformer as well as a single-phase full-wave rectifier. These two coils guided either SMF or ELF-PEMF through two iron blades (with 1-meter height and a cross-section of 10×10 cm^2).

A removable cell culture incubator (a plexiglass container with 35 cm length, 23 cm width and 52 cm height) as exposure unit was included between both iron blades (with 1 cm gap) as shown in **Supplementary Fig. S5b**, which was stabled by plastic bases upon wooden insulation (with 1 cm thickness), and exposure unit is above the coils with 15 cm distance. In the exposure unit, humidity, temperature (37 °C) and CO_2 atmosphere (5%) were controlled using three different sensors. To cool off the system, a gas chiller with optimum control on temperature was used. This automatic cooling system included an engine, an evaporator, a condenser, and a refrigerant gas (Freon-12). The engine is far enough from the exposure unit to avoid any significant MFs interference. The evaporator covered the outer surface of the coils, which enabled it to cool the system down effectively.

Overall cells were exposed to either sham or MFs conditions. Cells in sham-exposed conditions were incubated inside the not-energized coils in absence of MFs exposure. The effects of current-induced heating were not observed in the exposure unit **(Supplementary Fig. S6)**. The temperature was measured

inside and outside of the exposure unit, and external of the coils by thermometer at sham- and MFs-exposed conditions at different currents of DC and AC.

The exposure system was designed to generate continuously homogeneous either SMF in the range of 0.5 mT to 90 mT or ELF-PEMF at a frequency of 50 Hz in the stable conditions. An electronic board was used to stabilize the exposure system, therefore a SMF or ELF-PEMF were obtained inside of the exposure unit. A Teslameter (13610.93, PHYWE, Gottingen, Germany) with a probe-type of Hall Effect was used to measure MFs, calibrate the system and uniformity of MFs. A Hall Effect sensor is a transducer with the varying output voltage in response to MFs. Presence of any pulsation in the different currents were tested by an oscilloscope (40 MHz, model 8040, Leader Electronics Co., Yokohama, Japan), which resulted from rectifier into MFs exposure system. This pulsation frequency may be related to the shortcoming of single-phase full-wave rectifier used in the experiment, which provided a ripple voltage ~ 5%. However, the ripple voltage is not zero, it is small enough to confirm that generated MFs is highly homogeneous.

As seen in **Supplementary Fig. S5c**, the homogeneity of generated MFs was theoretically estimated by Complete Technology for 3D Simulation (CST STUDIO 2011 software) to select the best site for our samples within the exposure unit (http://www.CST.com). The profile of field emission in coils is demonstrated with surfaces of the same color. The local value of GMF in our lab was 47 ± 5 μT, according to measurement was performed by Tehran Geomagnetic Observatory, Institute of Geophysics, University of Tehran.

Detection of intracellular ROS generation

Intracellular ROS contents of HEK 293T cells were quantified using 2',7'-dichlorofluorescein diacetate (DCFDA) assay kit (ab113851, Abcam). For ROS assay, the 10×10^3 cells were seeded per well into 96-well plates by 100 μL supplemented DMEM and prepared for transfection and treatments, respectively. After that, cells were prepared immediately as manufacturer's recommendations. Briefly, the media was removed and cells were washed with PBS. Then, working DCFDA solution (20 μM DCFDA into 1X buffer) was added to each well upon the cells and incubated for 45 min at 37 ºC in the dark. The working solution was freshly made before each trial and did not store. After that, the buffer was completely removed, and rewashed and replaced with PBS. The measurement of ROS levels were monitored immediately by Cytation™ v3.0 Cell Imaging Multi-Mode Reader (BioTek, USA) at excitation / emission wavelengths of 485 / 535 nm.

Cell cycle analysis

Cell cycle distribution of HEK 293T cells was characterized using propidium iodide (PI) staining (Sigma-Aldrich). Briefly, the 150×10^3 cells were seeded per well into 6-well plates by 2 mL supplemented DMEM and prepared for transfection and treatments, respectively. After that for the assay, the medium was initially collected and cells were washed with PBS and trypsinized. Then, cells were rewashed twice with ice-cold PBS and centrifuged at 1200 rpm for 5 min. Supernatant was carefully removed, and cells were fixed by 70% (v/v) cold ethanol (Merck), then incubated at 4 °C overnight. Next, ethanol was removed and

cells were rewashed with cold PBS twice, carefully. Then, cells were resuspended in 50 µg/ml RNase-supplemented cold PBS and incubated at 37 °C for 1 h. After that, cell suspension was stained with a 50 µg/mL PI solution in PBS supplemented with 0.1% (v/v) Triton X-100 at room temperature for 1 h in the dark. Finally, cell cycle analysis was quantified immediately by FACSCalibur flow cytometer (Becton-Dickinson, Franklin Lakes, NJ). Data were collected from at least 10^4 cells and analyzed using FlowJo™ v10.6.2 software (FlowJo LLC, USA).

Cell viability experiments

The cell viability of HEK 293T cells was determined using tetrazolium salt ((3-(4,5-dimethylthiazol-2-yl)-2,5-diphenyltetrazolium bromide [MTT]) (Sigma-Aldrich). For MTT assay, the 10×10^3 cells were seeded per well into 96-well plates by 100 µL supplemented DMEM and prepared for transfection and treatments, respectively. After that, the media was removed and added 100 µL dye solution (0.5 mg/mL in FBS-free DMEM) to each well, and incubated at 37 °C for extra 4 h in the dark. The mitochondrial succinate dehydrogenases are able reduce the MTT to formazan as an indicator of cellular viability. Finally, the supernatants were removed and 100 µL Dimethyl sulfoxide (DMSO) (Daejung Chem., Korea) was added to each well and incubated for dissolve of formazan crystals. Then, the optical density (OD) of each well was quantified by a microplate reader (uQuant MQX200, BioTek, USA) at 570 nm. The percentage of cell viability was calculated based on the intensity of formazan compared to untreated cells (either control or sham) using standard formula as shown in **Eq. (1)**.

$$\text{Cell viability}(\%) = \frac{\text{OD}[\text{Treated cells} - \text{Blank cells}]}{\text{OD}[\text{Untreated cells} - \text{Blank cells}]} \times 100 \qquad (1)$$

Quantification of gene expression

Total cellular RNA was isolated from HEK 293T cells using a RiboEx reagent (GeneAll, Korea) according to the manufacturer's protocol. Briefly, the 150×10^3 cells were seeded per well into 6-well plates by 2 mL supplemented DMEM and prepared for transfection and treatments, respectively. After that, total RNA was extracted and quantified at 260/230 nm and 260/280 nm ratios indicated the yield of extracted RNA by a UV spectrophotometer (NanoDrop 2000c, Thermo Scientific, USA). RNA integrity was confirmed using an agarose gel electrophoresis. The cDNA synthesis was performed according to the following protocol: (1) DNase-1 treatment at 37 °C for 30 min to avoid genomic DNA contamination then followed by inactivation at 72 °C, (2) For mRNA reverse transcription enhancement, random hexamer and oligo dT mix primers were used, (3) cDNA synthesis was performed using the Prime Script II reverse transcriptase (Takara, Japan) at 42 °C for 70 min followed by RT inactivation at 72 °C for 12 min. Then, quantitative real-time PCR (qRT-PCR) was performed using high ROX SYBR® Green master mix assay kit (Biofact biofactory, Korea) by a StepOne™ Thermocycler (Applied Biosystems, USA). The primers were designed by oligoanalyzer software and, were synthesized by Pishgam Biotech Co. (Tehran, Iran). The quality of the qRT–PCR reactions was confirmed by melting curve analyses. The qRT–PCR data were calculated using

the comparative C_t method. The sequences of qRT-PCR forward (Fwd) and reverse (Rev) primers to amplify the fragments of OGG1 (173 bp), MTH1 (180 bp) and ITPA (167 bp) genes were respectively:

OGG1-Fwd, 5'-ACCCTGGCTCAACTGTATCACCAC-3';

OGG1-Rev, 5'-CCGCTCCACCATGCCAGTGATG – 3';

MTH1-Fwd, 5'-TGGGCCAGATCGTGTTTGAGTTCGT – 3';

MTH1-Rev, 5'-TCGTCGGGCCACATGTCCTTG-3';

ITPA-Fwd, 5'-AAGAAGCTGGAGGAGGTCG-3';

ITPA-Rev, 5'-TCCAAGGGCATTGAAGCACA-3';

GAPDH-Fwd, 5'-CCATGAGAAGTATGACAAC-3';

GAPDH-Rev, 5'-GAGTCCTTCCACGATACC-3'.

Expression data were normalized to the housekeeping gene of GAPDH as reference gene, which generated a 115 bp fragment to control the variability in expression levels. Reference gene was approximately equal in all experiments. The fold-change values were calculated for each time point.

Statistical analysis

GraphPad Prism v6.07 (GraphPad Software Inc., San Diego, CA) was used for statistical analysis and data graphing. We were applied one-way, (3 × 2) and (3 × 2 × 2) factorial ANalysis Of VAriance (ANOVA) followed by post-hoc analysis using Newman–Keuls multiple comparison test to compare between independent variables (e.g., cell type, DOX, SMF and EMF) in the ROS production, cell cycle distribution, cell viabilities, and gene expression. The error bars represent the mean ± standard deviation (SD) of at least three independent experiments (n = 3) for all biological-measured parameters in graphs. For all experiments: *$p < 0.05$; **$p < 0.001$; ***$p < 0.0001$, and $\alpha, p < 0.05$; $\beta, p < 0.01$; $\chi, p < 0.001$ were considered as a statistical significance difference.

Declarations

Data availability

All data generated or analyzed during this study are included in this published article and its supplementary information files.

Acknowledgments

The authors would like to thank the Research Council of Tarbiat Modares University. This study was financially supported by grant No. 960201 of the Biotechnology Development Council of the Islamic

Republic of Iran.

Author contributions

B.H.V. designed the experiments and performed, analyzed the data and also wrote the original draft. Moz.A. performed the experiments and analyzed the data. P.A. as corresponding author conducted research, sponsored the study and made all the arrangements. S.H. and M.K. conceived the study and methodology. Z.P., Moh.A. and N.R.A. coordinated the project and methodology. All authors contributed to the study design and reviewed the manuscript.

Competing interests

The authors declare no competing interests.

References

1. Van Huizen, A. V. *et al.* Weak magnetic fields alter stem cell–mediated growth. *Science advances.* **5**, eaau7201 (2019).
2. Elhalel, G., Price, C., Fixler, D. & Shainberg, A. Cardioprotection from stress conditions by weak magnetic fields in the Schumann Resonance band. *Scientific reports.* **9**, 1–10 (2019).
3. Baillet, S. Magnetoencephalography for brain electrophysiology and imaging. *Nature neuroscience.* **20**, 327–339 (2017).
4. Juutilainen, J., Herrala, M., Luukkonen, J., Naarala, J. & Hore, P. Magnetocarcinogenesis: is there a mechanism for carcinogenic effects of weak magnetic fields? Proceedings of the Royal Society B: Biological Sciences 285, 20180590 (2018).
5. Hore, P. J. Upper bound on the biological effects of 50/60 Hz magnetic fields mediated by radical pairs. *Elife.* **8**, e44179 (2019).
6. Touitou, Y. & Selmaoui, B. The effects of extremely low-frequency magnetic fields on melatonin and cortisol, two marker rhythms of the circadian system. *Dialogues in clinical neuroscience.* **14**, 381 (2012).
7. Zhu, X. *et al.* Moderate static magnetic fields enhance antitumor CD8 + T cell function by promoting mitochondrial respiration. *Sci. Rep.* **10**, 1–16 (2020).
8. Ahmed, I., Istivan, T., Cosic, I. & Pirogova, E. Evaluation of the effects of extremely low frequency (ELF) pulsed electromagnetic fields (PEMF) on survival of the bacterium Staphylococcus aureus. *EPJ Nonlinear Biomedical Physics.* **1**, 5 (2013).
9. Ehnert, S. *et al.* Translational Insights into Extremely Low Frequency Pulsed Electromagnetic Fields (ELF-PEMFs) for Bone Regeneration after Trauma and Orthopedic Surgery. *Journal of clinical medicine* **8**, 2028 (2019).
10. Wang, H. & Zhang, X. Magnetic fields and reactive oxygen species. *International Journal of Molecular Sciences.* **18**, 2175 (2017).

11. Verdom, B. H., Abdolmaleki, P. & Behmanesh, M. The static magnetic field remotely boosts the efficiency of doxorubicin through modulating ROS behaviors. *Scientific reports.* **8**, 1–12 (2018).
12. Timmel, C. R., Till, U., Brocklehurst, B., Mclauchlan, K. A. & Hore, P. J. Effects of weak magnetic fields on free radical recombination reactions. *Mol. Phys.* **95**, 71–89 (1998).
13. Rodgers, C. T. & Hore, P. J. Chemical magnetoreception in birds: the radical pair mechanism. Proceedings of the National Academy of Sciences 106, 353–360 (2009).
14. Nießner, C. & Winklhofer, M. Radical-pair-based magnetoreception in birds: radio-frequency experiments and the role of cryptochrome. *Journal of Comparative Physiology A.* **203**, 499–507 (2017).
15. Binhi, V. N. & Prato, F. S. Biological effects of the hypomagnetic field: An analytical review of experiments and theories. *PLoS One.* **12**, e0179340 (2017).
16. Qin, S. *et al.* A magnetic protein biocompass. *Nature materials.* **15**, 217–226 (2016).
17. Kattnig, D. R. & Hore, P. The sensitivity of a radical pair compass magnetoreceptor can be significantly amplified by radical scavengers. *Scientific reports.* **7**, 1–12 (2017).
18. Chaves, I. *et al.* The cryptochromes: blue light photoreceptors in plants and animals. *Annual review of plant biology.* **62**, 335–364 (2011).
19. Zoltowski, B. D. *et al.* Chemical and structural analysis of a photoactive vertebrate cryptochrome from pigeon. Proceedings of the National Academy of Sciences 116, 19449–19457 (2019).
20. Wang, Q. & Lin, C. Mechanisms of cryptochrome-mediated photoresponses in plants.*Annual Review of Plant Biology***71** (2020).
21. Kattnig, D. R., Solov'yov, I. A. & Hore, P. Electron spin relaxation in cryptochrome-based magnetoreception. *Physical Chemistry Chemical Physics.* **18**, 12443–12456 (2016).
22. Kattnig, D. R. Radical-pair-based magnetoreception amplified by radical scavenging: resilience to spin relaxation. *The Journal of Physical Chemistry B.* **121**, 10215–10227 (2017).
23. Giachello, C. N., Scrutton, N. S., Jones, A. R. & Baines, R. A. Magnetic fields modulate blue-light-dependent regulation of neuronal firing by cryptochrome. *Journal of Neuroscience.* **36**, 10742–10749 (2016).
24. Shostak, A. Circadian clock, cell division, and cancer: from molecules to organism. *International journal of molecular sciences.* **18**, 873 (2017).
25. Xie, Y. *et al.* New insights into the circadian rhythm and its related diseases. *Frontiers in physiology.* **10**, 682 (2019).
26. Feillet, C., Van Der Horst, G. T., Levi, F., Rand, D. A. & Delaunay, F. Coupling between the circadian clock and cell cycle oscillators: implication for healthy cells and malignant growth. *Frontiers in neurology.* **6**, 96 (2015).
27. Ozturk, N., Ozturk, D., Kavakli, I. H. & Okyar, A. Molecular aspects of circadian pharmacology and relevance for cancer chronotherapy. *International journal of molecular sciences.* **18**, 2168 (2017).

28. Rossi, E., Corsetti, M. T., Sukkar, S. & Poggi, C. Extremely low frequency electromagnetic fields prevent chemotherapy induced myelotoxicity. *Electromagnetic Biology and Medicine.* **26**, 277–281 (2007).
29. Kaszuba-Zwoinska, J. *et al.* Pulsating electromagnetic field stimulation prevents cell death of puromycin treated U937 cell line. *Journal of Physiology and Pharmacology.* **61**, 201 (2010).
30. Guerra, M. F., Lacoste, M. G., Anzulovich, A. C. & Makinistian, L. Magnetic fields, cancer and circadian rhythms: hypotheses on the relevance of intermittence and cycling. Proceedings of the Royal Society B 286, 20192337 (2019).
31. Wyszkowska, J., Shepherd, S., Sharkh, S., Jackson, C. W. & Newland, P. L. Exposure to extremely low frequency electromagnetic fields alters the behaviour, physiology and stress protein levels of desert locusts. *Scientific reports.* **6**, 36413 (2016).
32. Kapri-Pardes, E. *et al.* Activation of signaling cascades by weak extremely low frequency electromagnetic fields. *Cellular Physiology and Biochemistry.* **43**, 1533–1546 (2017).
33. Kalyanaraman, B. Teaching the basics of the mechanism of doxorubicin-induced cardiotoxicity: Have we been barking up the wrong tree?. *Redox Biol.* **29**, 101394 (2020).
34. Zhu, H. *et al.* Doxorubicin redox biology: redox cycling, topoisomerase inhibition, and oxidative stress. *Reactive oxygen species (Apex, NC).* **1**, 189 (2016).
35. Taymaz-Nikerel, H., Karabekmez, M. E., Eraslan, S. & Kırdar, B. Doxorubicin induces an extensive transcriptional and metabolic rewiring in yeast cells. *Scientific reports.* **8**, 1–14 (2018).
36. Cappetta, D. *et al.* Doxorubicin targets multiple players: a new view of an old problem. *Pharmacological research.* **127**, 4–14 (2018).
37. Clayton, F., Tessnow, K. A., Fang, J. C., Holden, J. A. & Moore, J. G. Circadian variation of topoisomerase II-α in human rectal crypt epithelium: implications for reduction of toxicity of chemotherapy. *Modern pathology.* **15**, 1191–1196 (2002).
38. Onishi, Y. & Kawano, Y. Rhythmic binding of Topoisomerase I impacts on the transcription of Bmal1 and circadian period. *Nucleic acids research.* **40**, 9482–9492 (2012).
39. Panieri, E. & Santoro, M. ROS homeostasis and metabolism: a dangerous liason in cancer cells. *Cell death & disease.* **7**, e2253–e2253 (2016).
40. Sies, H. & Jones, D. P. Reactive oxygen species (ROS) as pleiotropic physiological signalling agents.*Nature Reviews Molecular Cell Biology*,1–21(2020).
41. de Araújo, R. F., Martins, D. B. G. & Borba, M. A. C. in A master regulator of oxidative stress-the transcription factor nrf2 (IntechOpen, 2016).
42. Nadalutti, C. A. *et al.* Mitochondrial dysfunction and DnA damage accompany enhanced levels of formaldehyde in cultured primary human fibroblasts. *Scientific reports.* **10**, 1–13 (2020).
43. Mehta, J., Rayalam, S. & Wang, X. Cytoprotective effects of natural compounds against oxidative stress. *Antioxidants.* **7**, 147 (2018).
44. Souliotis, V. L. *et al.* DNA damage response and oxidative stress in systemic autoimmunity. *International Journal of Molecular Sciences.* **21**, 55 (2020).

45. Surova, O. & Zhivotovsky, B. Various modes of cell death induced by DNA damage. *Oncogene.* **32**, 3789–3797 (2013).
46. Perillo, B. *et al.* ROS in cancer therapy: the bright side of the moon.*Experimental & Molecular Medicine*,1–12(2020).
47. Dizdaroglu, M., Coskun, E. & Jaruga, P. Repair of oxidatively induced DNA damage by DNA glycosylases: Mechanisms of action, substrate specificities and excision kinetics. *Mutation Research/Reviews in Mutation Research.* **771**, 99–127 (2017).
48. Lee, T. H. & Kang, T. H. DNA oxidation and excision repair pathways. *International Journal of Molecular Sciences.* **20**, 6092 (2019).
49. Ghodbane, S., Lahbib, A., Sakly, M. & Abdelmelek, H. Bioeffects of static magnetic fields: oxidative stress, genotoxic effects, and cancer studies. BioMed research international 2013 (2013).
50. Kıvrak, E. G., Yurt, K. K., Kaplan, A. A., Alkan, I. & Altun, G. Effects of electromagnetic fields exposure on the antioxidant defense system. *Journal of microscopy and ultrastructure.* **5**, 167–176 (2017).
51. Sefidbakht, Y. *et al.* Effects of 940 MHz EMF on bioluminescence and oxidative response of stable luciferase producing HEK cells. *Photochem. Photobiol. Sci.* **13**, 1082–1092 (2014).
52. Yu, B., Choi, B., Li, W. & Kim, D. H. Magnetic field boosted ferroptosis-like cell death and responsive MRI using hybrid vesicles for cancer immunotherapy. *Nature communications.* **11**, 1–9 (2020).
53. Sancar, A. *et al.* Circadian clock control of the cellular response to DNA damage. *FEBS letters.* **584**, 2618–2625 (2010).
54. Lewczuk, B. *et al.* Influence of electric, magnetic, and electromagnetic fields on the circadian system: current stage of knowledge.*BioMed Research International***2014** (2014).
55. Channell, J. & Vigliotti, L. The role of geomagnetic field intensity in late quaternary evolution of humans and large mammals. *Reviews of Geophysics.* **57**, 709–738 (2019).
56. Price, C., Williams, E., Elhalel, G. & Sentman, D. Natural ELF fields in the atmosphere and in living organisms.*International Journal of Biometeorology*,1–8(2020).
57. Uebe, R. & Schüler, D. Magnetosome biogenesis in magnetotactic bacteria. *Nat. Rev. Microbiol.* **14**, 621 (2016).
58. Nordmann, G. C., Hochstoeger, T. & Keays, D. A. Magnetoreception—a sense without a receptor. *PLoS biology.* **15**, e2003234 (2017).
59. Krishnan, V. *et al.* Wireless control of cellular function by activation of a novel protein responsive to electromagnetic fields. *Scientific reports.* **8**, 1–12 (2018).
60. Sherrard, R. M. *et al.* Low-intensity electromagnetic fields induce human cryptochrome to modulate intracellular reactive oxygen species. *PLoS biology.* **16**, e2006229 (2018).
61. Hiscock, H. *et al.* Navigating at night: fundamental limits on the sensitivity of radical pair magnetoreception under dim light.*Quarterly reviews of biophysics***52** (2019).
62. Damulewicz, M. & Mazzotta, G. M. One actor, multiple roles: the performances of CRYPTOCHROME in Drosophila.*Frontiers in Physiology***11** (2020).

63. Dufor, T. *et al.* Neural circuit repair by low-intensity magnetic stimulation requires cellular magnetoreceptors and specific stimulation patterns. *Science advances.* **5**, eaav9847 (2019).
64. Gauger, M. A. & Sancar, A. Cryptochrome, circadian cycle, cell cycle checkpoints, and cancer. *Cancer research.* **65**, 6828–6834 (2005).
65. Sahar, S. & Sassone-Corsi, P. Metabolism and cancer: the circadian clock connection. *Nat. Rev. Cancer.* **9**, 886–896 (2009).
66. Terzibasi-Tozzini, E. & Martinez-Nicolas, A. & Lucas-Sánchez, A. in*Seminars in Cell & Developmental Biology.*164–176(Elsevier).
67. Hernández-Rosas, F., López-Rosas, C. A. & Saavedra-Vélez, M. V. Disruption of the molecular circadian clock and cancer: an epigenetic link. *Biochemical genetics.* **58**, 189–209 (2020).
68. Miki, T., Matsumoto, T., Zhao, Z. & Lee, C. C. p53 regulates Period2 expression and the circadian clock. *Nature communications.* **4**, 2444 (2013).
69. Marley, R., Giachello, C. N., Scrutton, N. S., Baines, R. A. & Jones, A. R. Cryptochrome-dependent magnetic field effect on seizure response in Drosophila larvae. *Scientific reports.* **4**, 5799 (2014).
70. Arthaut, L. D. *et al.* Blue-light induced accumulation of reactive oxygen species is a consequence of the Drosophila cryptochrome photocycle. *PLoS One.* **12**, e0171836 (2017).
71. Farshadi, E., van der Horst, G. T. & Chaves, I. Molecular Links between the Circadian Clock and the Cell Cycle.*Journal of Molecular Biology*(2020).
72. Manzella, N. *et al.* Circadian modulation of 8-oxoguanine DNA damage repair. *Scientific reports.* **5**, 13752 (2015).
73. Yudkina, A. V., Shilkin, E. S., Endutkin, A. V., Makarova, A. V. & Zharkov, D. O. Reading and misreading 8-oxoguanine, a paradigmatic ambiguous nucleobase. *Crystals.* **9**, 269 (2019).
74. Bridge, G., Rashid, S. & Martin, S. A. DNA mismatch repair and oxidative DNA damage: implications for cancer biology and treatment. *Cancers.* **6**, 1597–1614 (2014).
75. Van Houten, B., Santa-Gonzalez, G. A. & Camargo, M. DNA repair after oxidative stress: current challenges. *Current opinion in toxicology.* **7**, 9–16 (2018).
76. Görgens, H. *et al.* Analysis of the base excision repair genes MTH1, OGG1 and MUTYH in patients with squamous oral carcinomas. *Oral oncology.* **43**, 791–795 (2007).
77. Simone, P. D., Pavlov, Y. I. & Borgstahl, G. E. ITPA (inosine triphosphate pyrophosphatase): from surveillance of nucleotide pools to human disease and pharmacogenetics. *Mutation Research/Reviews in Mutation Research.* **753**, 131–146 (2013).
78. Ji, D. *et al.* Measuring deaminated nucleotide surveillance enzyme ITPA activity with an ATP-releasing nucleotide chimera. *Nucleic acids research.* **45**, 11515–11524 (2017).
79. Pokorny, R. *et al.* Recognition and repair of UV lesions in loop structures of duplex DNA by DASH-type cryptochrome. Proceedings of the National Academy of Sciences 105, 21023–21027 (2008).
80. Kang, T. H. & Leem, S. H. Modulation of ATR-mediated DNA damage checkpoint response by cryptochrome 1. *Nucleic acids research.* **42**, 4427–4434 (2014).

81. Bee, L. *et al.* Nucleotide excision repair efficiency in quiescent human fibroblasts is modulated by circadian clock. *Nucleic acids research.* **43**, 2126–2137 (2015).
82. Kochan, D. Z. *et al.* Circadian-disruption-induced gene expression changes in rodent mammary tissues. *Oncoscience.* **3**, 58 (2016).
83. Riancho, J. *et al.* The role of magnetic fields in neurodegenerative diseases.*International Journal of Biometeorology*,1–11(2020).
84. Cheraghi, R., Alipour, M., Nazari, M. & Hosseinkhani, S. Optimization of conditions for gene delivery system based on PEI. *Nanomedicine Journal.* **4**, 8–16 (2017).

Figures

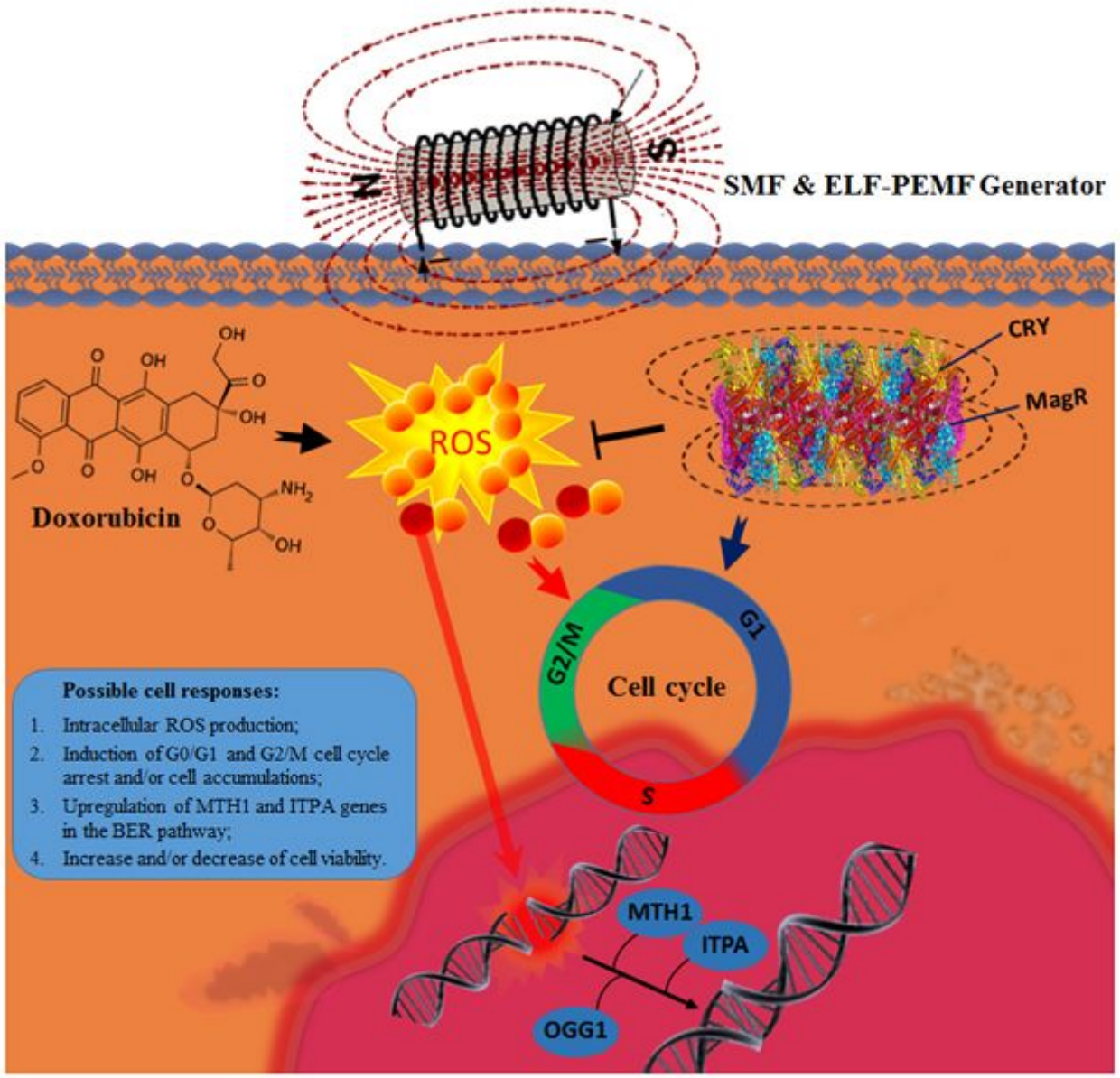

Figure 1

Schematic illustration of the possible physiological responses of cells overexpressing the cryptochrome (CRY)-based magnetosensitive proteins to intracellular levels of ROS due to doxorubicin treatment and wireless effects of homogeneous SMF and ELF-PEMF on the capacity of BER pathway and cell cycle progression. The rod-like shaped magnetosensor complexes is depended on coupling of CRY-photoreceptor proteins with putative magnetosensitive MagR proteins.

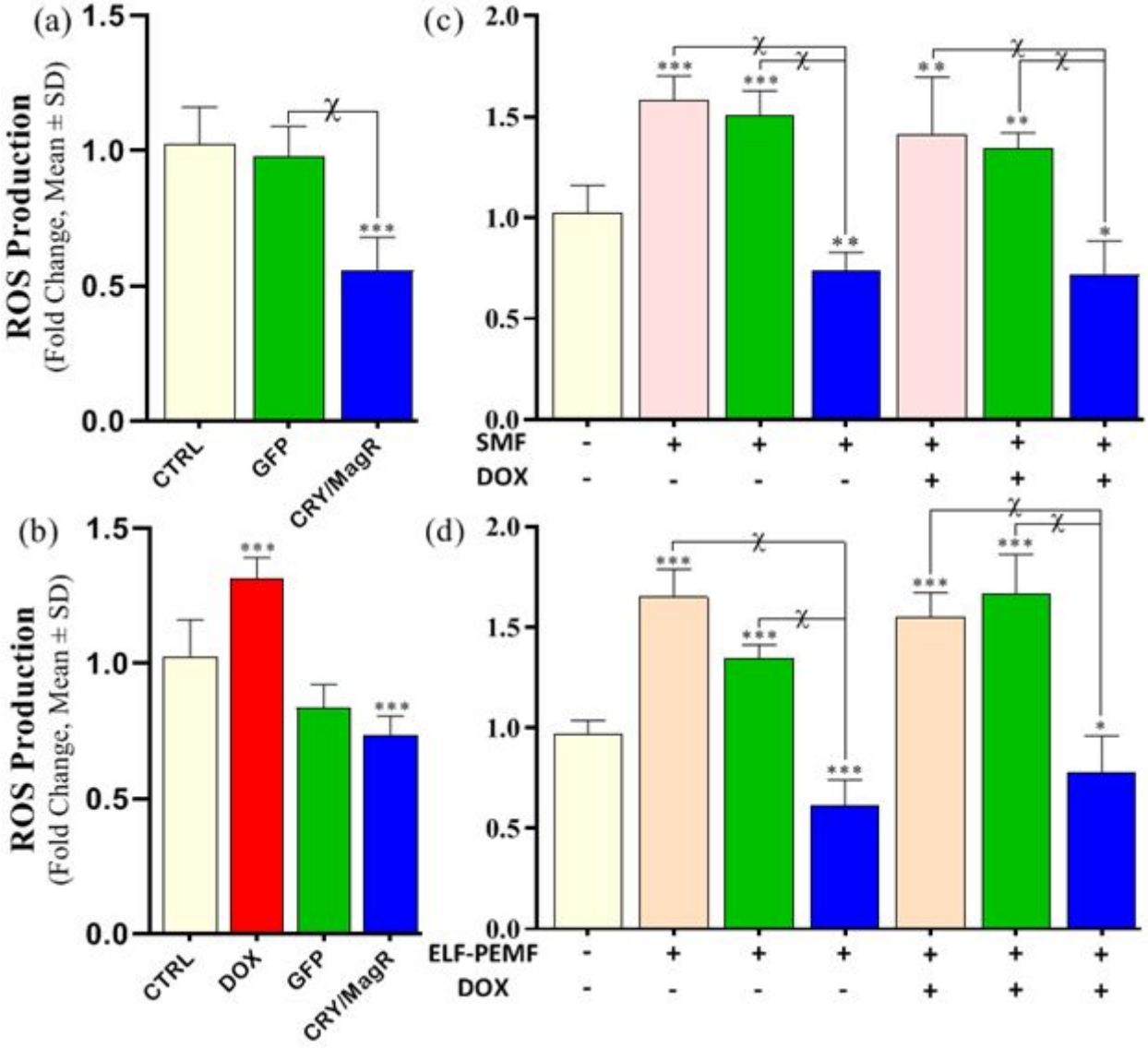

Figure 2

The intracellular ROS accumulation of HEK 293T cells expressing either GFP (green bars) or CRY/MagR (blue bars) at the (a) endpoint of transfection and 24 h after that in the (b) absence (-) and presences (+) of (c) SMF (15 mT) and (d) ELF-PEMF (50 Hz) treated with DOX (0.1 μM). The ROS concentrations were measured by DCFDA fluorescent probe and Cytation Cell Imaging Multi-Mode Reader. The results are expressed as a fold-value of unexposed cells (control (CTRL) and sham). Data are shown as the mean ± SD (n = 3 independent biological replicates). *p < 0.05; **p < 0.01; ***p < 0.001 show significant differences relative to either CTRL or sham, and letter (χ,p < 0.001) show significant differences between

treated cells, which were analyzed by one-way, (3 × 2) and (3 × 2 × 2) factorial ANOVA followed with post-hoc Newman–Keuls multiple comparison tests.

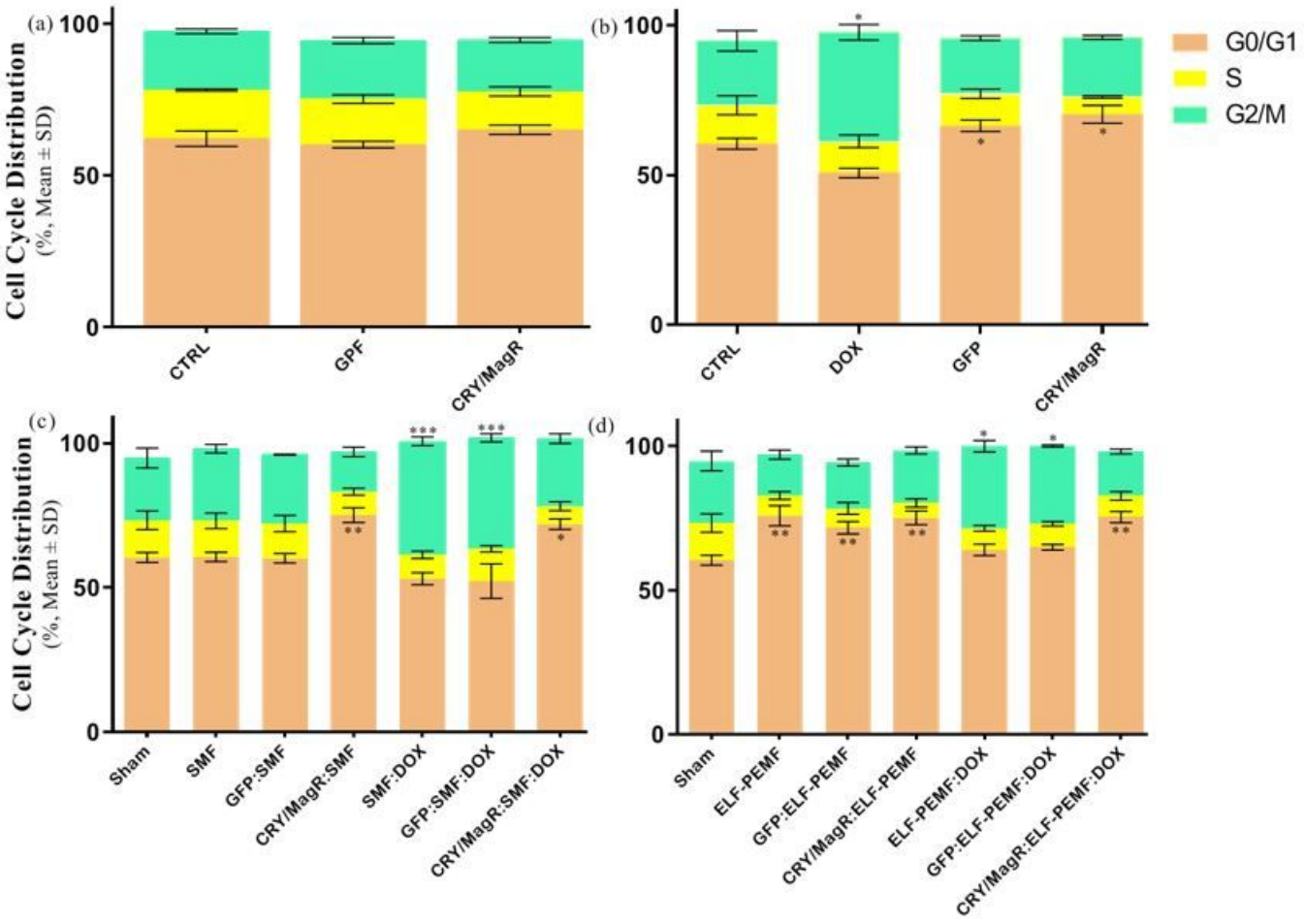

Figure 3

The cell cycle progression of HEK 293T cells expressing either GFP or CRY/MagR at the (a) endpoint of transfection and 24 h after that in the (b) absence and presences of (c) SMF (15 mT) and (d) ELF-PEMF (50 Hz) with DOX (0.1 μM) treatment. The representative results of cell cycle phase were analyzed by PI staining and flow cytometer assay. The results are expressed as percentage of unexposed cells (control (CTRL) and sham). Data are shown as the mean ± SD (n = 3 independent biological replicates). *p < 0.05; **p < 0.01; ***p < 0.001 show significant differences relative to either CTRL or sham, which were analyzed by one-way, (3 × 2) and (3 × 2 × 2) factorial ANOVA followed with post-hoc Newman–Keuls multiple comparison tests.

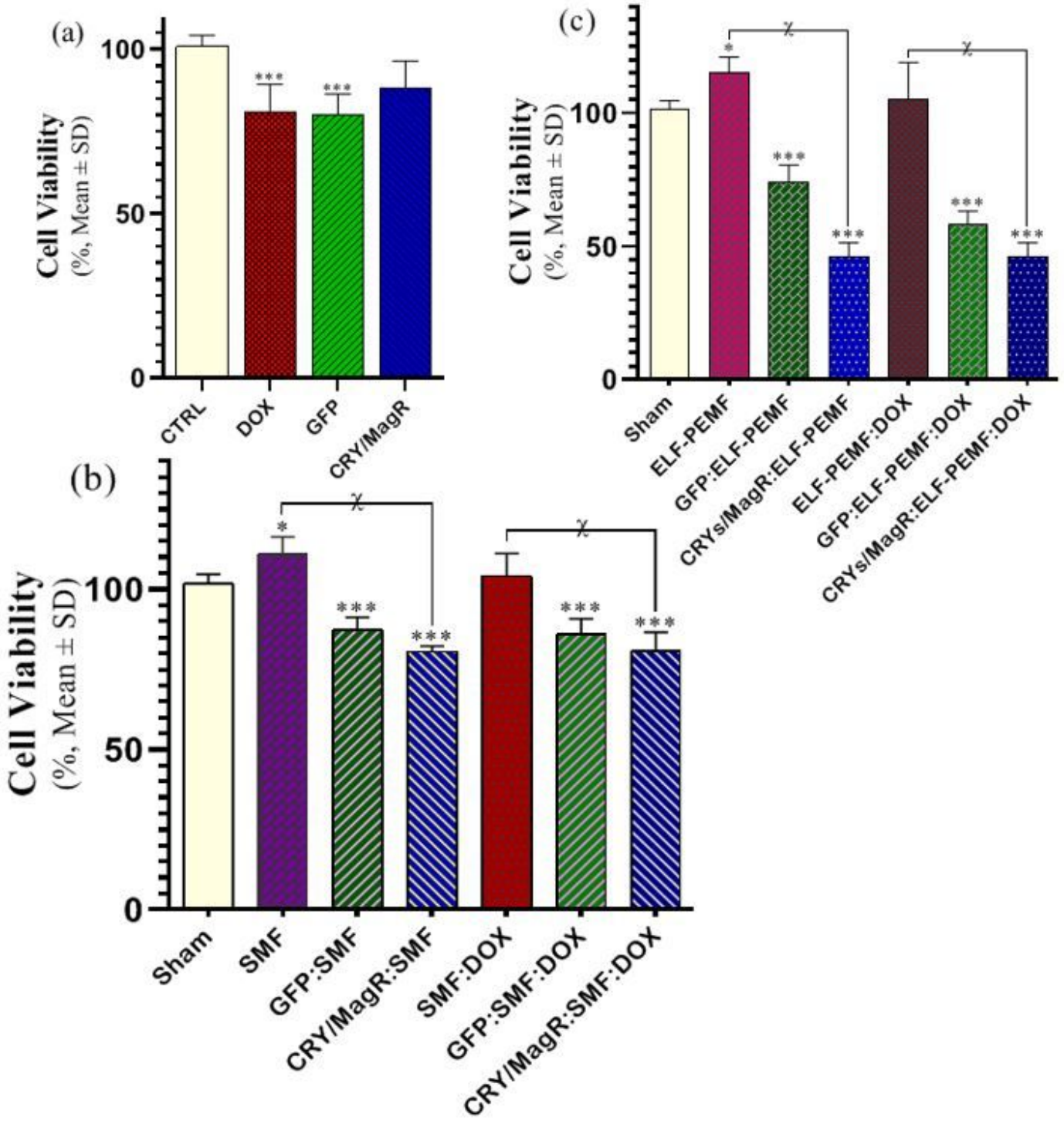

Figure 4

The cell viability of HEK 293T cells expressing either GFP (green bars) or CRY/MagR (blue bars) in the (a) absence and presences of (b) SMF (15 mT) and (c) ELF-PEMF (50 Hz) treated with DOX (0.1 μM) for 24 h post-transfection. Comparison of cell proliferation between the wild-type cells and treated cell groups were determined by MTT staining and microplate reader. MTT was added into cells to form the formazan, and DMSO was then added to dissolve the formazans. The optical density (OD) values of mixture were determined at 570 nm by a microplate reader. The results are expressed as percentage of viable cells in

the control (CTRL) or sham conditions. Data are shown as the mean ± SD (n = 3 independent biological replicates). *,P < 0.05; ***,P < 0.001 show significant differences relative to either CTRL or sham, and letters (χ,p < 0.001) show significant differences between treated cells, which were analyzed by (3 × 2) and (3 × 2 × 2) factorial ANOVA followed with post-hoc Newman–Keuls multiple comparison tests.

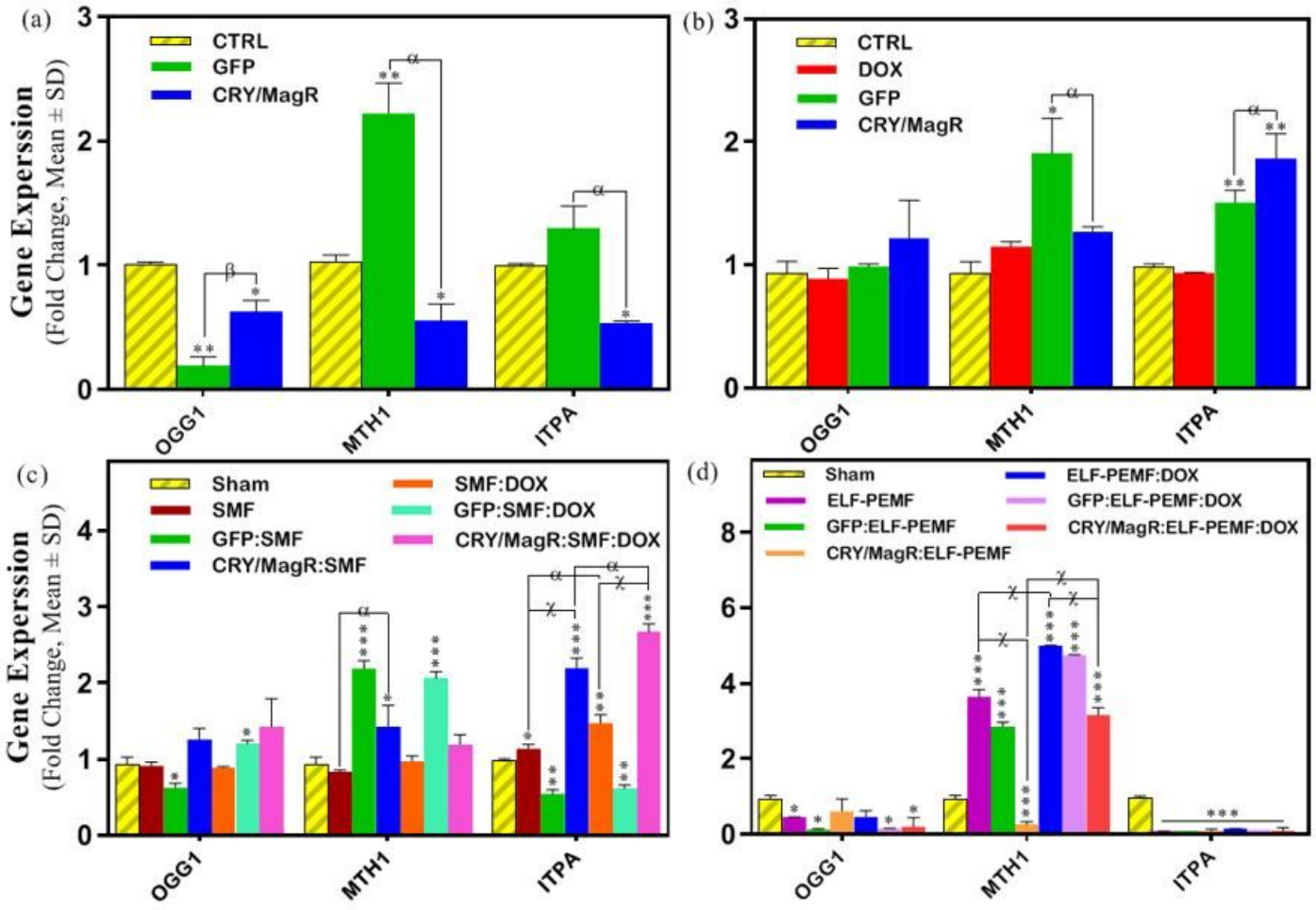

Figure 5

The relative mRNA expression level of oxidative stress-responsible genes in the HEK 293T cells expressing either GFP or CRY/MagR at the (a) endpoint of transfection and 24 h after that in the (b) absence and presences of (c) SMF (15 mT) and (d) ELF-PEMF (50 Hz) treated with DOX (0.1 μM). The quantification of oxidative-related gene expression levels including 8-oxoguanine DNA glycosylase-1 (OGG1), human mutt homolog 1 (MTH1) and inosine triphosphate pyrophosphate (ITPA) were determined by qRT-PCR analysis. The results are expressed as a fold-value of untreated cells (control (CTRL) and sham). Data are shown as the mean ± SD (n = 3 independent biological replicates). *p < 0.05; **p < 0.01; ***p < 0.001 show significant differences relative to either CTRL or sham, and letters (α,p < 0.05; β,p < 0.01; χ,p < 0.001) show significant differences between treated cells, which were analyzed by one-way, (3 × 2) and (3 × 2 × 2) factorial ANOVA followed with post-hoc Newman–Keuls multiple comparison tests. (***; refers to the all cell groups).

Supplementary Files

This is a list of supplementary files associated with this preprint. Click to download.

- SupplementaryInformation.pdf